Absorption and diffusion of oxygen in the Ti3Al alloy

Article *in* Journal of Experimental and Theoretical Physics · July 2017

DOI: 10.1134/S1063776117070019

CITATIONS
2

READS
58

3 authors:

Alexander V. Bakulin
Institute of Strength Physics and Materials Science, Siberian Branch of Russian Acad…
53 PUBLICATIONS **139** CITATIONS
SEE PROFILE

Alexander Michailovich Latyshev
National Research University Higher School of Economics
7 PUBLICATIONS **5** CITATIONS
SEE PROFILE

Svetlana Kulkova
Institute of Strength Physics and Materials Science of the Siberian Branch of Siberia…
152 PUBLICATIONS **856** CITATIONS
SEE PROFILE

ISSN 1063-7761, Journal of Experimental and Theoretical Physics, 2017, Vol. 125, No. 1, pp. 138–147. © Pleiades Publishing, Inc., 2017.
Original Russian Text © A.V. Bakulin, A.M. Latyshev, S.E. Kulkova, 2017, published in Zhurnal Eksperimental'noi i Teoreticheskoi Fiziki, 2017, Vol. 152, No. 1, pp. 164–176.

ORDER, DISORDER, AND PHASE TRANSITION IN CONDENSED SYSTEM

Absorption and Diffusion of Oxygen in the Ti_3Al Alloy

A. V. Bakulin*[a], A. M. Latyshev[a], and S. E. Kulkova[b,]**

[a] *Institute of Strength Physics and Material Science, Siberian Branch, Russian Academy of Sciences, Tomsk, 634055 Russia*

[b] *National Research Tomsk State University, Tomsk, 634050 Russia*

**e-mail: bakulin@ispms.tsc.ru*

***e-mail: kulkova@ms.tsc.ru*

Received February 28, 2017

Abstract—The absorption and diffusion of oxygen in the Ti_3Al alloy are studied by the projector augmented wave within the density functional theory. The highest absorption energies are shown to correspond to the sites in the octahedra formed by six titanium atoms, and the presence of aluminum in the nearest neighbors leads to a substantial decrease in the binding energy of oxygen in the alloy by approximately 1.5 eV. The energy barriers of oxygen diffusion between various interstices in the crystal lattice of the alloy are estimated, and the preferred migration paths in the (0001) plane and the [0001] direction are determined. It is found that the migration barrier from the most preferred octahedral O1 site to distorted tetrahedral Ti-site (2.42 eV) is a key barrier and limits the oxygen diffusion in the alloy. The calculated temperature diffusion coefficient of oxygen in the Ti_3Al alloy and the activation energies determined in two directions agree with the experimental data.

DOI: 10.1134/S1063776117070019

1. INTRODUCTION

The high-temperature oxidation of titanium and its alloys is known to cause the formation of oxide films of various compositions on their surfaces [1]. When oxygen interacts with pure titanium, a double oxide layer with a rutile structure forms on its surface [2]. The formation of a compact inner oxide layer having equiaxed grains is considered to be an effective barrier of oxygen diffusion into the material. Alloying of titanium with various elements (Al, Sn, Mo, Zr, Ta, Nb, etc.), even with a set of elements, improves its functional properties. Titanium aluminides are considered as the most promising structural materials for the aviation, aerospace, and automobile industries due to their low density, high strength at various temperatures, and good creep resistance [1, 3]. However, insufficient corrosion resistance of Ti_3Al and TiAl alloys limits their application at high temperatures [1, 4–6]. Although $TiAl_3$ has the best corrosion properties among the Ti–Al alloys, it is a rather brittle material because of its low symmetry.

The addition of aluminum to titanium makes the process of its oxidation more complex, since both components of the alloy have an affinity for oxygen. It is the formation of a dense oxide layer with a corundum α-Al_2O_3 structure on the surfaces of alloys with a low titanium content ensures their high corrosion resistance. It is known that the chemical activity of aluminum decreases with increasing titanium content [1, 4, 5]; in combination with the thermodynamic characteristics of oxides, this feature implies a higher stability of interfaces with TiO and TiO_2 than with Al_2O_3. The growth of mixed oxide layers was experimentally detected on the surfaces of the Ti_3Al and TiAl alloys, and the outer layers of the oxide films, which are not in contact with the alloys, undergo cracking and partial spallation [1, 6, 7]. The development of new titanium aluminide-based materials, the mechanical properties of which will be between the properties of nickel-based superalloys and high-temperature ceramics, is a challenging problem of modern materials science. Therefore, it is necessary to control the structure and properties of the surface layers in Ti–Al alloys and the conditions of their oxidation. This problem implies theoretical studies of the interaction of oxygen with a surface and its diffusion in alloys of various compositions.

The authors of [8] performed a comparative investigation of the initial stage of oxidation of the surfaces of the Ti_3Al and TiAl alloys at 650°C and showed that this process of oxidation can be divided into three stages. At the first stage, oxygen molecules adsorb and dissociate and atomic oxygen penetrates into the subsurface layers of the alloys. This stage terminates when

the surface and subsurface layers are saturated by oxygen, and this preoxidation process is more pronounced in the Ti_3Al alloy due to a higher oxygen solubility [8].

At the second stage, the alloy undergoes selective oxidation and aluminum oxide islands form on its surface, which can result from the surface segregation of aluminum. In this connection, we note work [9], where the microscopic mechanisms of oxidation of the $Ti_3Al(0001)$ surface were studied theoretically. An analysis of the energy stability of the surface at various defect concentrations and oxygen coverages showed that the $Ti_3Al(0001)$-3Al surface with three aluminum defects in the titanium sublattice (Al antisite) in the surface layer was more stable in the Al-rich limit. In addition, oxygen adsorption was found to enhance the aluminum segregation to the alloy surface. The formation of aluminum oxide on the alloy surface leads to the formation of a titanium-rich region and, hence, an increase in the chemical activity of titanium [8].

When the titanium concentration reaches a critical value, the third stage begins. It is characterized by simultaneous growth of titanium and aluminum oxides: a TiO_2 film forms on the alloy surface and an Al_2O_3 film, at the alloy–TiO_2 interface. As was found in [8], the diffusion of Ti^{3+} titanium cations to the surface through aluminum oxide is possible because of its imperfection.

Note that the second stage of oxidation is characterized by a parabolic law, which corresponds to the existence of an effective barrier to oxygen diffusion, which decelerates oxidation. At the third stage, the reaction rate increases and the oxidation kinetics deviates from a parabolic law [8]. It was noted in a number of works (see, e.g., [10]) that adsorption takes place on surface titanium atoms and the chemisorption rate decreases when the aluminum concentration in the alloy increases. Moreover, the kinetics of oxidation of Ti–Al alloys, especially at low temperatures, is mainly determined by the growth mechanisms of an oxide scale, i.e., diffusion, rather than surface processes. However, the contrary standpoint also exists [11].

Thus, information on the energy barriers and the oxygen diffusion mechanisms in metals and alloys is important to better understand their oxidation and the effect of alloying impurities on this process. A low diffusion rate and a high activation energy are known to be favorable for high-temperature structural materials. Although the diffusion of light elements in metals and alloys and the self-diffusion and diffusion of impurities are being extensively studied by various experimental techniques (see, e.g., [12–19] and Refs. therein), the results obtained are still contradictory. The scatter of the temperature diffusion coefficients and the diffusion activation energies is substantial. It is known that a number of problems related to the purity of a sample, the possibilities of radiotracer elements, and surface oxidation, arise during an experimental estimation of the temperature diffusion coefficients in materials.

The density functional theory (DFT) in combination with the transition state theory [20, 21] makes it possible to understand the mechanisms of diffusion of interstitial and substitutional impurities and the mechanisms of self-diffusion in metallic systems and compound with various crystal structures on a microscopic level. As a result, the number of works, where the diffusion of interstitial atoms is studied by the DFT methods, increases rapidly [22–32]. Most works deal with the calculation of hydrogen diffusion in various metallic systems. The diffusion of oxygen in metals with a hexagonal structure was systematically investigated in [32]. Alloys have received little attention as compared to metals, and hydrogen diffusion was mainly studied [26–30]. The oxygen adsorption on the surfaces of Ti–Al alloys was mainly investigated in dependence on their orientation and termination [33–41], and the γ-TiAl alloy has received the most study [33–37]. In [38], we considered the adsorption on surface of an aluminum-rich $TiAl_3$ alloy. Moreover, we also investigated the oxygen diffusion from the surface of a TiAl alloy into its bulk [36, 37] and the oxygen diffusion in bulk TiAl and $TiAl_3$ alloys [36, 38, 39].

It should be noted that interest in the Ti_3Al alloy is caused by the fact that, in contrast to $TiAl_3$, it has a high strength in a wide temperature range. Therefore, its electronic structure and the effect of alloying impurities on its mechanical properties were repeatedly studied in recent years [42–44]. The authors of [40] investigated the adsorption of molecular oxygen on the stoichiometric $Ti_3Al(0001)$ surface, and in [41] they analyzed the adsorption of atomic oxygen on the same surface. They showed that an oxygen adatom predominantly forms bonds with titanium atoms, as in other Ti–Al alloys.

It is known that the preferred location of an oxygen atom at a certain site does restrict its diffusion. Moreover, diffusion in metals and alloys can be anisotropic, which is also related to the atomic environment of interstitial sites. As far as we know, there is only one work where the diffusion of oxygen in the Ti_3Al alloy was studied by oxygen implantation and Auger electron spectroscopy in the temperature range 723–1073 K [19]. The authors of [19] obtained almost the same activation energies along axes c and a, 187.3 kJ/mol (1.94 eV) and 184.8 kJ/mol (1.92 eV), respectively. They also obtained similar values using a theoretical estimation with the formulas from [45] and several sets of adjustable parameters. To the best of our knowledge, no DFT calculations of the barriers of oxygen diffusion in the Ti_3Al alloy were carried out.

The purpose of this work is to perform an ab initio theoretical investigation of the absorption and diffusion of oxygen in the Ti_3Al alloy.

2. CALCULATION PROCEDURE

The atomic and electronic structures of the Ti_3Al alloy were calculated by the projector augmented wave (PAW) method in a plane wave basis [46, 47] using the VASP program code [48, 49] and the generalized gradient approximation for an exchange-correlation functional in the GGA-PBE form [50]. The plane-wave cut-off energy from a basis set was 550 eV. In the electronic structure calculation, the integration over the Brillouin zone was performed using a Γ-centered $13 \times 13 \times 17$ grid of k points. Convergence was considered to be achieved when the difference between the total energies of the two last iterations did not exceed 10^{-5} eV. Atomic positions were relaxed using the Newton dynamics until the force at an atom was at most 0.01 eV/Å. We used a full relaxation scheme to optimize a cell; it also included changes in the cell volume and shape.

The absorption energy of an oxygen atom was calculated by the formula

$$E_{abs} = -[E_{O/Ti_3Al} - E_{Ti_3Al} - E_{O_2}/2], \quad (1)$$

where E_{O/Ti_3Al} and E_{Ti_3Al} ate the total energies of the alloy with and without oxygen, respectively, and E_{O_2} is the total energy of the oxygen molecule calculated in an empty cell with sides of $12 \times 12 \times 12$ Å. Factor 1/2 corresponds to the absorption of one oxygen atom in the alloy. To calculate the absorption energy in a $(1 \times 1 \times 1)$ cell, we used a $7 \times 7 \times 9$ grid of k points, and a $3 \times 3 \times 4$ grid of k points was used in the case of a $(2 \times 2 \times 2)$ cell.

To estimate the diffusion barriers of oxygen in the Ti_3Al alloy, we applied the climbing image nudged elastic band method [51]. The initial position of five images along an elementary path was found by linear interpolation between the initial and final positions of a diffusing atom. During subsequent simultaneous relaxation of all five images, each atom was assumed to be elastically bound to the same atom in the neighboring images. This model allows us to accurately determine the trajectory with the minimum energy and the point with the maximum energy, which is called a saddle point. The energy barrier to the migration of an oxygen atom along this trajectory was estimated as the difference between the total energies of the alloy with oxygen in the initial and saddle positions. Note that an increase in the number of points in the irreducible part of the Brillouin zone, namely, the use of $4 \times 4 \times 5$ and $5 \times 5 \times 6$ cells of k points, leads to a change in the energy barrier by 0.03 eV. Test calculations also showed that the migration barriers remained almost unchanged when the plane-wave cut-off energy increased from 550 to 650 eV. On the whole, the accuracy of the energy barrier calculations was 0.05 eV.

3. RESULTS AND DISCUSSION

3.1. Structural and Electronic Properties of Ti_3Al

The Ti_3Al alloy is known to have a hexagonal close-packed $D0_{19}$ structure (Fig. 1a). It is characterized by space group 194, where titanium and aluminum are located at sites $6h$ and $2c$ according to the Wyckoff classification. The calculated lattice parameters of the alloy ($a = 5.736$ Å and $c = 4.639$ Å) differ from the experimental values ($a = 5.770$ Å and $c = 4.616$ Å [52]) by less than 0.6%. Note that the calculated elastic modulus ($B = 119$ GPa) agrees well with the experimental value (113 GPa [53]) and the elastic constants ($C_{11} = 193$, $C_{12} = 90.7$, $C_{13} = 66.6$, $C_{33} = 235.8$, $C_{44} = 55.5$, $C_{66} = 51.1$ GPa) differ from the experimental values [53] by 5–10%, which is allowable in such calculations.

The electron energy spectrum and the density of states (DOS) of the alloy, which are shown in Figs. 1b and 1c, also agree well with those presented in [42–44]. It is seen that the low-energy states in the energy range from −7.5 to −5 eV are mainly caused by the s-states of aluminum and the p-states dominate up to −5 eV, and their contribution at the Fermi level is significantly lower than that of the d-states of titanium. The position of the Fermi level near a local minimum in the DOS curve indicates that this structure is stable. The main contribution to bonding states is due to the hybridization of the Ti-d–Ti-d states, since they mainly form the occupied part of the valence band in the energy range from −5 to 0 eV (Fig. 1c). The covalent character of bonding, which is caused by the hybridization Al-p–Ti-d in this energy range, is less pronounced. Thus, the chemical bond in the alloy mainly has a metallic character.

3.2. Oxygen Absorption in the Ti_3Al Alloy

The Ti_3Al alloy is characterized by two types of octahedral sites having different compositions of the nearest environment (Fig. 1a): O1 is at the center of the octahedron formed by six titanium atoms, and O2 is at the center of the octahedron formed by four titanium atoms and two aluminum atoms. All tetrahedral sites are formed by three titanium atoms and one aluminum atom, which can be located in the base of the tetrahedron in the basal plane (T1) or at its vertex (T2). Table 1 gives the calculated energies of oxygen absorption in the unit cell of the alloy and in the cell doubled in three directions. Site O1 is seen to be preferable for oxygen sorption in the bulk.

The neutron diffraction experiments performed in [54] also demonstrate that oxygen atoms tend to occupy titanium-rich octahedral sites. The presence of aluminum in the nearest neighbors leads to a substantial (by 1.47 eV) decrease in the absorption energy at site O2. Almost the same values were obtained in [55] using the pseudopotential method. By definition, a higher absorption energy means stronger bonding of

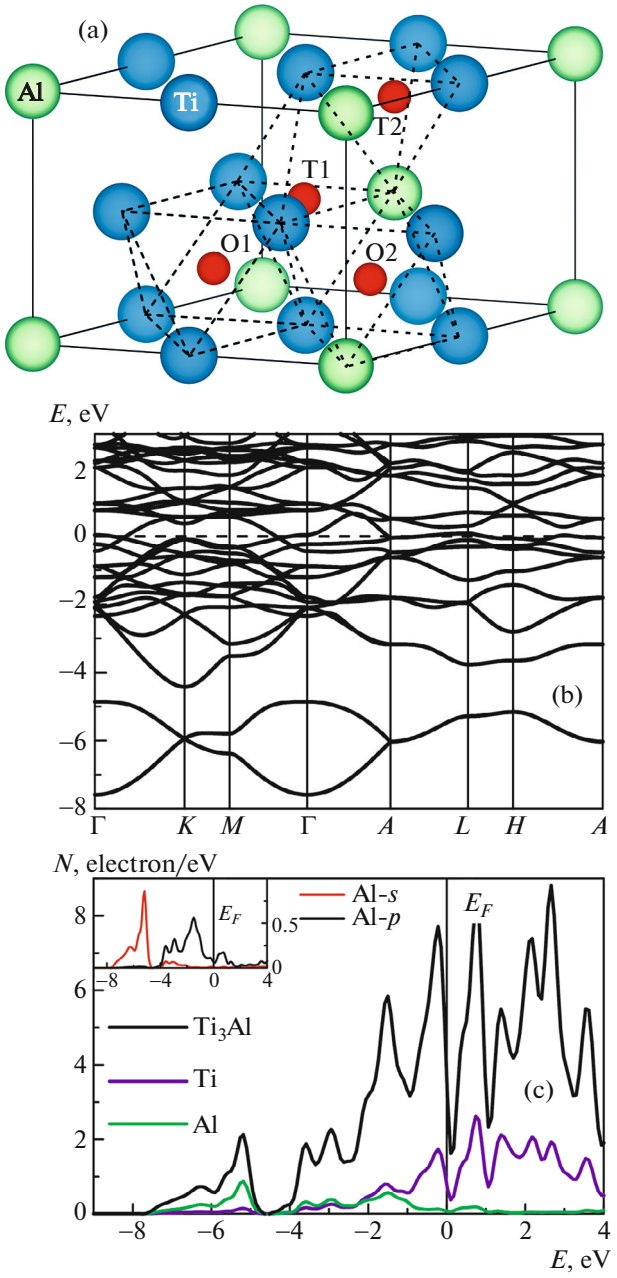

Fig. 1. (Color online) Unit cell of the Ti_3Al alloy: (a) octahedral (O) and tetrahedral (T) sites (small balls) for oxygen absorption, (b) electronic energy spectrum, and (c) total and local DOSs.

oxygen to matrix atoms. It is seen from Table 1 that, as the cell size increases, the absorption energy in octahedral sites changes by at most 0.06 eV.

The incorporation of oxygen in the lattice of the alloy is known to induce local distortions. In this work, lattice optimization included a change in the cell shape along with a change in the cell volume and atomic site relaxation. The change in the cell shape is most pronounced for a small cell and this effect

Table 1. Oxygen absorption energy E_{abs} and the structural (ΔV, $\Delta c/a$, d) and electronic (Δq) characteristics of the Ti_3Al alloy

Site	O1	O2	T1	T2
E_{abs} (1 × 1 × 1), eV	6.22	4.68	4.58	3.77
E_{abs} (2 × 2 × 2), eV	6.16	4.69	4.24	3.78
Theory [55] E_{abs}, eV	6.23	4.75	4.20	3.83
ΔV (1 × 1 × 1), %	2.56	3.50	6.44	10.05
ΔV (2 × 2 × 2), %	0.36	0.48	0.88	1.21
$\Delta c/a$ (1 × 1 × 1), %	0.05	0.74	−11.75	−4.72
$\Delta c/a$ (2 × 2 × 2), %	−0.01	0.10	−1.13	−0.60
d(O–Ti), Å	2.10	2.07	1.93	1.92
d(O–Al), Å	3.52	2.08	1.88	1.91
Δq(O), el.	1.28	1.51	1.39	1.35
Δq(Ti), el.	−0.20	−0.10	−0.15	−0.02
Δq(Al), el.	–	−0.51	−0.66	−0.64

decreases with increasing cell size. Although the cell shape does not change during the oxygen incorporation in our case, the c/a ratio changes. This effect ($\Delta c/a$ in Table 1) is most pronounced for T1-site, where the results obtained for two cells change by more than 0.3 eV. Note that an oxygen atom shifts from the center of an octahedron to its base and occupies the so-called hexahedral site in the basal plane at the center of the triangle formed by two titanium atoms and one aluminum atom (see Fig. 1a). In [25], this site in pure titanium was called a basal tetrahedral site. We do not introduce a new designation for this site and consider it as a distorted tetrahedral site.

As is seen from Table 1, the oxygen absorption energy at T1-site is lower than that at O2-site by 0.45 eV (0.55 eV [55]). Note that the tetrahedral sites in pure titanium are unstable for oxygen; therefore, during relaxation they shift toward the hexahedral sites, the energy at which is lower than that at the octahedral sites by 1.19 eV [32]. This difference in the Ti_3Al alloy reaches 1.92 eV. However, during absorption at T2-site (which differs in the location of aluminum in a tetrahedron), oxygen is retained at its center, in contrast to pure titanium. The lower oxygen absorption energies at the tetrahedral sites correlate with a large change in the cell volume; that is, oxygen can hardly be incorporated in these sites because of smaller interstice volume. On the whole, an analysis of the oxygen absorption energies in all titanium aluminides (TiAl [36], $TiAl_3$ [38]) demonstrates that oxygen tends to occupy titanium-rich sites irrespective of the aluminide composition.

Figure 2 shows the charge density difference calculated by the formula

$$\Delta\rho = \rho_{tot} - \sum_i \rho_{at}^i,$$

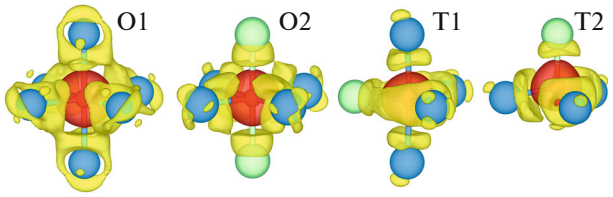

Fig. 2. (Color online) Charge density difference distribution for oxygen adsorption at octahedral and tetrahedral sites. (red) Charge accumulation region and (yellow) charge depletion region.

where ρ_{tot} is the total electron density of the system with oxygen at sites O or T, ρ_{at}^{i} is the atomic electron density, and the sum is taken over all atoms in the cell. It is seen that the electron density accumulates near an oxygen atom for all sites, whereas the charge goes from the nearest atoms of the metallic matrix. The charge distribution in all sites shown in Fig. 2 reflects the ionic mechanism of oxygen bonding in the Ti_3Al alloy. The charge transfer calculation by the Bader method (see Table 1) showed that a charge $\Delta q = 1.3–1.5$ electrons goes to oxygen from the nearest atoms, depending on the type of interstitial site. The substitution of titanium atoms by two aluminum atoms during the absorption of oxygen at O2-sites leads to a decrease in the charge transfer from titanium atoms, each of the four atoms loses a charge of about 0.1 electron, and a high charge up to 0.5 electrons comes to oxygen from aluminum. Recall that part of the charge accumulates in the Ti–Al bond due to its covalence.

The less charge transfer from titanium to oxygen is caused by stronger localization of its *s*-, *d*-states as compared to the delocalized *s*-, *p*-states of aluminum. In sites T1 and T2, the charge coming to oxygen from aluminum is almost the same, and titanium atoms lose a higher charge (about 0.15 electrons) in the former case (see Table 1). Although the charge transfer is minimal at site O1 (which indicates a lower ionic contribution to the chemical bond of oxygen with the alloy matrix), the stronger hybridization of the *s*-, *p*-orbitals of oxygen with the *s*-, *d*-orbitals of a transition metal as compared to the *s*-, *p*-orbitals of aluminum causes its preference. This hybridization contribution becomes substantially weaker when aluminum appears in the nearest environment of an oxygen atom, which is clearly visible from the local DOS distribution shown in Fig. 3.

The valence band of oxygen is seen to consist of two subbands, the sharp peak in the energy range from –21 to –20 eV is caused by *s*-orbitals, and the wider *p*-band extends to –8 eV. Small peaks of the states of Ti and Al, which are induced by interaction with the *s*-orbitals of oxygen, also exist at these energies, and the peaks of Al are absent for absorption at O1-site. Recall that the nearest aluminum atom for which DOSs are shown in Fig. 3a is a next nearest neighbor of oxygen located at

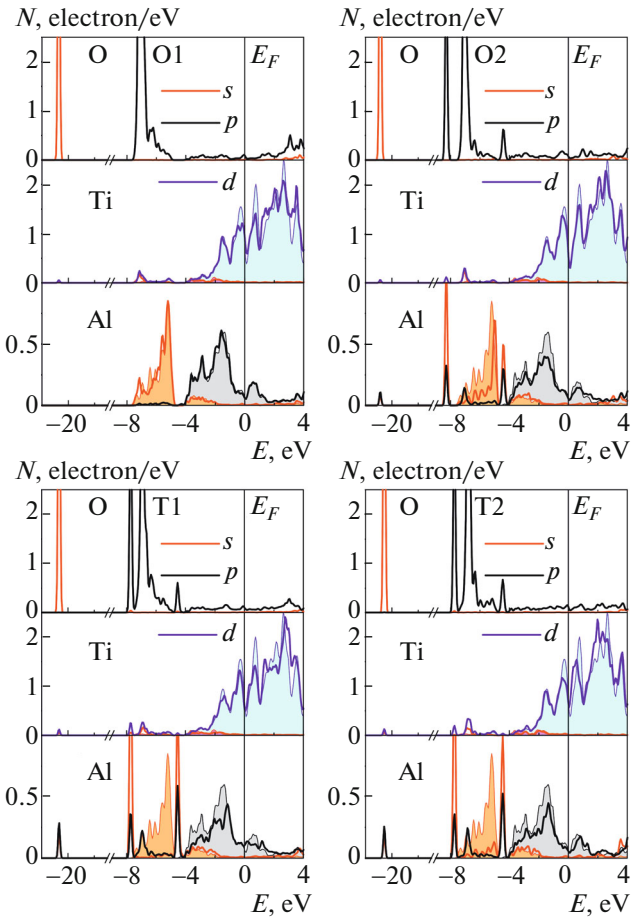

Fig. 3. (Color online) Partial DOSs of oxygen and the nearest titanium and aluminum atoms at octahedral (O1, O2) and tetrahedral (T1, T2) sites. The DOSs of titanium and aluminum atoms in the oxygen-free alloy are shadowed.

a distance of 3.52 Å. In this case, the DOSs of Al change insignificantly because of the indirect interaction induced by the hybridization of the *s*-, *p*-states of aluminum with the *s*-, *d*-states of titanium, which are directly involved in the chemical bond with oxygen. The strong hybridization of the *s*-, *d*-states of titanium with the *p*-states of oxygen at O1-site results in the appearance of split-off states near the metallic valence band bottom at energies from –7.5 to –5 eV, and these states were absent in the DOSs of these atoms in the alloy. The increase in the number of states with high energies leads to their decrease near the Fermi level. The changes in the DOS of aluminum are more pronounced for oxygen absorption at O2-site. Apart from a small peak at an energy of –20.8 eV, the DOS of Al has a sharp peak in the range from –9 to –8 eV, which is mainly generated by the *s*-states of aluminum. Moreover, split-off *p*-states of aluminum appear in the energy range from –7 to –4 eV, and the energy positions of the peaks coincide with the peaks from the *p*-band of oxygen. The change in the states of titanium

at O2-site is similar to that described above for O1-site.

Since the Ti–O and Al–O bond lengths for the tetrahedral sites are smaller than for the octahedral sites, the interaction of oxygen with these atoms becomes stronger. The split-off states of titanium and aluminum are located at an energy of –20.7 eV and in the range from –8 to –4 eV. The appearance of these states points to the formation of new O–Ti and O–Al bonds and evidences a weakening of the Ti–Al bonds in the alloy. On the whole, the energy position of the fine structure of the DOS peaks of metals coincides with that of the corresponding peaks of the *s*-, *p*-states of oxygen. Although the interaction of oxygen with metals is stronger in the tetrahedral sites (which is seen from the increase in the number of metallic states involved in this interaction), the decrease in the number of the nearest metallic atoms brings about a decrease in the binding energy of oxygen at these sites.

3.3. Temperature Coefficient of Diffusion and Activation Energy

We now consider the diffusion of an oxygen atom along the trajectories that are possible in the Ti_3Al alloy (Fig. 4). All migration paths of an oxygen atom can be divided into the following three groups: I, along the [0001] direction; II, in the (0001) basal plane; and III, the paths that lie between sites in different basal planes and are not one below another exactly. Table 2 gives the energy barriers calculated along the paths shown in Fig. 4. The highest energy barrier obtained for oxygen diffusion between the O1-sites in the [0001] direction is 3.48 eV, which is higher than the barrier (3.02 eV) for the O1 → O1 jump in the TiAl alloy [36] and is substantially higher than the value (2.05 eV) obtained by us for $TiAl_3$ [38]. Thus, despite the differences in the symmetries of the crystal lattices of Ti–Al alloys, the energy barrier of oxygen diffusion from these sites increases with increase of the titanium content near an oxygen atom.

The calculated diffusion barrier between octahedral O1-sites is higher than the corresponding barrier in α-Ti (3.25 eV [32]), which was calculated by the pseudopotential method with use of the generalized gradient approximation. Note that the methods used to calculate the total energy in this work and in [32] give similar results. The difference in the energy barriers (0.23 eV) agrees with the experimental data (0.1–0.2 eV) [19]. The higher barrier between the energy preferable sites for oxygen absorption in Ti_3Al in comparison with α-Ti points to a lower diffusivity of oxygen in the alloy, which is consistent with the experimental data in [19, 56–60].

Although the barrier of oxygen diffusion along the O2 → O2 path in the [0001] direction is lower than for O1 → O1 (see Table 2), an oxygen has to spend higher energy to penetrate into O2-site (it is necessary to add the difference between the energies at sites O1 and O2 to the migration barrier), which makes the diffusion between O2-sites less preferred. Note that the oxygen migration along the T2 → T2 path in the [0001] direction is characterized by a low barrier (0.20 eV). However, this path does not correspond to translation invariance and can only be considered as part of the complex path, e.g., O2 → T2 → T2 → O2.

Table 2. Oxygen migration barriers in the Ti_3Al alloy (E_m, eV). The barriers for the back diffusion are given in square brackets

I	O1 → O1	O2 → O2	T2 → T2
	3.48	2.33	0.20
II	O1 → O2	O2 → O2	T1 → T1
	2.97 [1.50]	1.44	1.87
III	O1 → T1	O2 → T1 (O2 → T2)	T1 → T1 (T1 → T2)
	2.42 [0.50]	1.31 [0.85] (1.38 [0.47])	0.79 (1.09 [0.63])

The barriers of oxygen migration between the octahedral sites in the basal plane were found to be slightly lower than those along the [0001] direction (see Table 2), whereas the energy barrier between the tetrahedral sites increases. In the latter case, a saddle point is located between two atoms (in an edge of octahedron), which increases the energy at this site. The energy barriers of oxygen diffusion along the paths of the third type (O1 → T1, O2 → T1, or O2 → T2) are also rather high and exceed the corresponding barriers in TiAl and $TiAl_3$ alloys by approximately 1 eV. Since the tetrahedral sites are less preferable, the reverse diffusion requires lower energy (see Table 2).

On the whole, an analysis of our results allows us to conclude that the path O1 → T1 → O1 is the most preferred oxygen diffusion path in the [0001] direction (Figs. 5a, 5b). Diffusion in the perpendicular direction occurs along the trajectory O1 → T1 → O2 → O2 → T1 → O1 and can pass from one basal plane to another

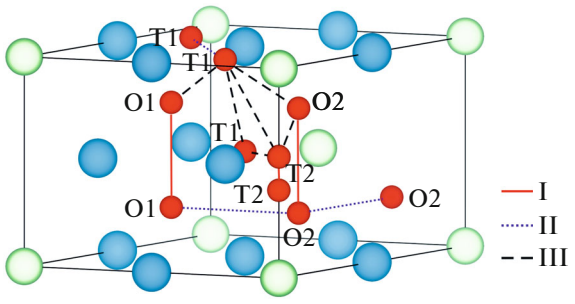

Fig. 4. (Color online) Oxygen migration paths in the Ti_3Al alloy between various interstitial sites. The designation of atoms is identical to that in Fig. 1.

(Figs. 5a, 5c). In all cases, the highest barrier of oxygen diffusion in the alloy at a low oxygen concentration is 2.42 eV, which corresponds to the elementary path O1 → T1 (Figs. 5b, 5c). As in the case of the TiAl alloy, titanium-rich sites can be traps for oxygen, which hinders the formation of bonds between oxygen and aluminum atoms and retards its diffusion. Note that the corresponding energy barrier in the TiAl alloy is almost half as much (1.15 eV [36]).

Let us dwell on the temperature diffusion coefficient of oxygen in the Ti_3Al alloy, $D = D_0\exp(-E_a/k_BT)$. The authors of [19] were the first to measure it, and they also calculated it using a technique that is an extension of the theory proposed in [45] to describe the oxygen diffusion in α-Ti. In that technique, they took into account the frequencies of oxygen atom jumps along various elementary paths using the activation energy of each path and the multiplicities of oxygen interstitial sites. Three different calculations were performed and based on the following assumptions: (i) the oxygen energy at O1-site was taken to be zero; (ii) oxygen atom jump frequency ν along all elementary paths was assumed to be the same and calculated by the formula

$$\nu = \sqrt{\frac{Q}{2md^2}}. \qquad (2)$$

A frequency of $\nu = 3.28 \times 10^{11}$ s^{-1} was obtained in [19] for the following parameters: diffusion activation energy Q along axis a is 185 kJ/mol, the oxygen atom mass is $m = 2.66 \times 10^{-26}$ kg, and the path length is $d = c/2 = 0.232$ nm. In the first (simplest) case, the authors of [19] used the same energy for an oxygen atom in the tetrahedral sites and the same energy for all saddle points and did not take into account the influence of the nearest neighbors. In the second model, the energies at interstitial sites were determined using the hard sphere model. In the third model, they took the experimental values of activation energy for saddle points, namely, $Q = 187$ kJ/mol (1.94 eV) for jumps between O sites and $Q = 185$ kJ/mol (1.92 eV) for forward and backward O → T jumps. Moreover, one of the parameters, namely, the energy of oxygen at site O2 (E_{O2}), was varied in all three calculations. The activation energy in Eq. (2) was determined by the difference between the energies at O1-site and the corresponding saddle point, i.e., $E_s - E_{O1}$.

On the whole, the authors of [19] achieved good agreement between the calculated and experimental data for some values of the variational parameters, in particular, for $E_{O2} = 5$ kJ/mol in the first model and when this value was zero in the third model. An insignificant anisotropy of the diffusion coefficient was detected for these cases. However, conflicting conclusions regarding diffusion anisotropy were also drawn depending on a model and the parameter to be varied. It should also be noted that an error was made in [19] when calculating frequency ν by Eq. (2). The frequency at the parameters given above is significantly

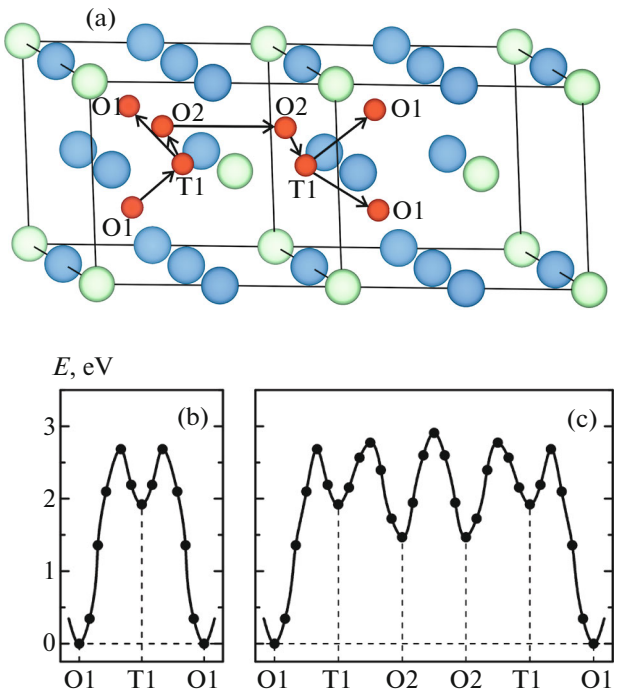

Fig. 5. (Color online) (a) Octahedral and tetrahedral absorption sites of a oxygen atom in the Ti_3Al alloy and the preferred paths of its migration along axes c and a and the diffusion profiles of preferred diffusion paths along (b) [0001] direction and in (c) (0001) plane. The designation of atoms is identical to that in Fig. 1.

higher (10.37×10^{12} s^{-1}). In this case, the calculated values illustrated by the dashed line in Fig. 6a lie well above the experimental values. Note that the experimental data obtained by different techniques can differ by one–two orders of magnitude, since they are strongly affected by the purity of samples, lattice defects, and many other factors. Therefore, the same difference between calculated and experimental results is considered to be allowable.

In contrast to [19], we calculated the temperature diffusion coefficient using a specific value of ν for each elementary jump and the corresponding energy barriers and paths in Eq. (2). The frequency of an oxygen atom jump from site i to site j taking into account the temperature was calculated by the following formula:

$$\Gamma_{i\to j} = \nu_{i\to j}\exp\left(-\frac{E_m^{i\to j}}{k_BT}\right), \qquad (3)$$

where $E_m^{i\to j}$ is the barrier of oxygen migration along the path $i \to j$, k_B is the Boltzmann constant, and T is the temperature. The average jump time was estimated by the formula

$$\tau_{i\to j} = \frac{1}{\Gamma_{i\to j}}. \qquad (4)$$

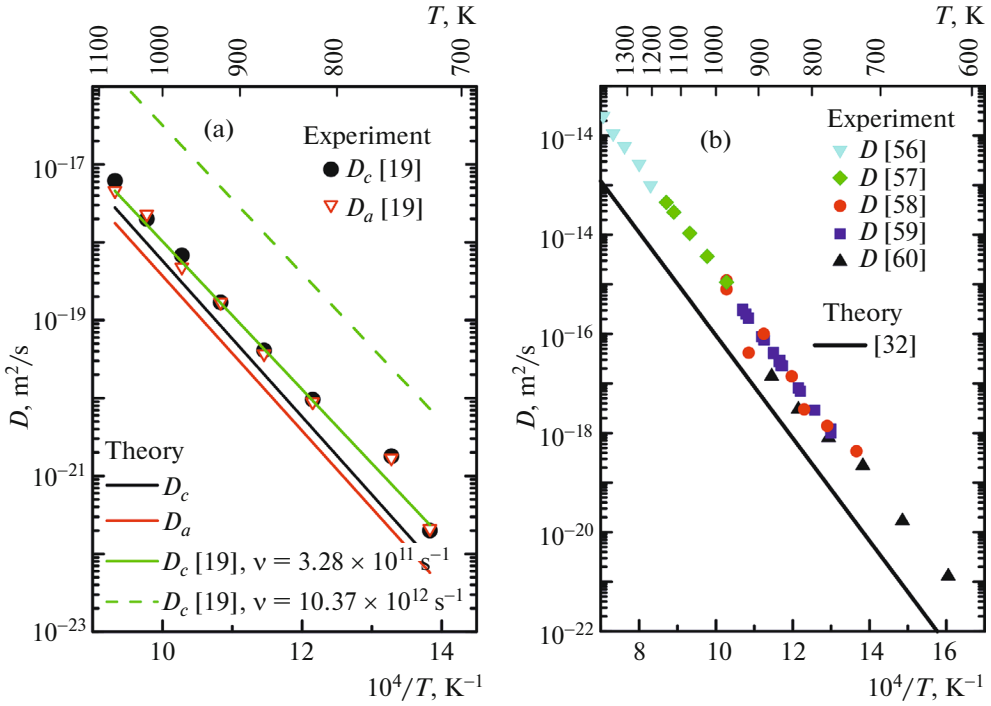

Fig. 6. (Color online) Calculated and experimental diffusion coefficients of oxygen in (a) Ti_3Al alloy and (b) α-Ti.

The $i \to j$ jump probability was written as the ratio of the jump frequency to the sum of the frequencies of all transitions from site i with allowance for their multiplicity $n_{i \to k}$,

$$P_{i\to j} = \frac{\Gamma_{i\to j}}{\sum\limits_k n_{i\to k}\Gamma_{i\to k}}. \qquad (5)$$

The probability of the fact that an initial site is occupied by an oxygen atom was calculated by the formula

$$F_i = \frac{n_i \exp(E^i_{\text{abs}}/k_BT)}{\sum\limits_k n_k \exp(E^k_{\text{abs}}/k_BT)}, \qquad (6)$$

where n_k is the multiplicity of interstitial site k.

Thus, with allowance for all quantities described above, the temperature diffusion coefficient for the path $i \to j$ takes the form

$$D_{i\to j} = F_i n_i \left(\frac{\mathbf{u}\cdot\mathbf{s}}{|\mathbf{u}|}\right)^2 \frac{\prod\limits_k P_{i\to k}}{\sum\limits_k \tau_{i\to k}}, \qquad (7)$$

where $\mathbf{s}$ is the diffusing atom displacement vector and $\mathbf{u}$ is the vector of an arbitrary length directed along crystal axis a or c. The resulting diffusion coefficient is the sum of all such coefficients. The product and the sum in the numerator and the denominator of Eq. (6) appear when we consider diffusion along a path consisting of several elementary parts. In this case, the probability of such a complex path is calculated as the product of the probabilities of the corresponding elementary jumps, and the average migration time is calculated as the sum of the corresponding times. Therefore, we may omit long paths, since the total probability of such an event decreases significantly when the number of jumps increases. Note that the oxygen diffusion paths along directions a and c, which were discussed above (see Fig. 5), are the most probable paths for oxygen migration between preferred O1 sites from one unit cell to another.

As is seen from Fig. 6a, the temperature diffusion coefficient calculated by the described procedure using the energy barriers obtained within the DFT agrees well with the experimental data from [19]. Since no other experimental results for the Ti_3Al alloy are available, in Fig. 6b we present the experimental [56–60] and calculated [32] data on the temperature diffusion coefficient of oxygen in α-Ti. The experimental data are seen to have a scatter, and, hence, different activation energies (1.75–2.14 eV) were obtained. Moreover, only the average activation energy can be experimentally obtained, whereas the barriers for all elementary paths, which differ from the average values, can be theoretically calculated (see Table 2). The diffusion coefficients in pure titanium [32] calculated by the procedure from [51] within the DFT using energy bar-

riers also differ from the experimental data by approximately an order of magnitude (Fig. 6b). Note that activation energies calculated from the temperature diffusion coefficient of oxygen in the Ti_3Al alloy along axes *a* and *c* are 1.99 and 1.97 eV, respectively. The obtained activation energies agree well with the experimental data (1.94 and 1.92 eV, respectively [19]). The small diffusion anisotropy along the two directions also agrees with the conclusion drawn from experimental data in [19]. An analogous conclusion was made in [32] using the theoretical calculations of α-Ti. These results imply that the rate of oxygen diffusion along the [0001] direction is only weakly higher than that in the basal plane.

On the whole, both the model calculations [19] and our ab initio estimates demonstrate that the diffusion coefficient of oxygen in the alloy is lower than that in pure titanium. The oxygen–titanium bonds in the Ti_3Al alloy are considered to be weaker than those in pure titanium because of the covalent character of the titanium–aluminum bond, which causes lower activation energies in the alloy. Since the lattice parameters of the alloy differ insignificantly from those of titanium, this geometric factor should not substantially affect the oxygen diffusion rate. Therefore, the lower oxygen diffusion rate in the alloy can be caused by the fact that the number of preferred O1 sites for oxygen sorption decreases fourfold as compared to titanium. Six of the eight possible octahedral sites are the O2 sites where the oxygen absorption energy is substantially lower than at O1-sites. Moreover, the key barrier to the O1 → T1 diffusion in titanium is lower than that in the alloy by approximately 0.4 eV, and the number of possible preferred jumps is higher. Thus, a smaller number of preferred diffusion paths in the Ti_3Al alloy causes a decrease in the oxygen diffusion rate as compared to that in pure titanium.

4. CONCLUSIONS

The absorption of oxygen in the Ti_3Al alloy was calculated by the PAW method within the DFT. The oxygen absorption was shown to be preferable at titanium-rich O1 octohedral sites. The site in the tetrahedron with titanium at its vertex is unstable, since, as in pure titanium [32], an oxygen atom shifts toward the base of the tetrahedron and occupies the hexahedral site in the basal plane. The appearance of aluminum in the nearest neighbors leads to a decrease in the binding energy of oxygen in the Ti_3Al alloy, which agrees with the tendencies found earlier for other titanium aluminides [36, 38, 55] and the experimental data from [54].

The calculation of the barriers for oxygen diffusion in the Ti_3Al alloy showed that the indirect oxygen diffusion mechanism between octahedral O1-sites through intermediate T1-site (O1 → T1 → O1) is preferred along the [0001] direction as compared to the direct O1 → O1 jump. The migration of oxygen atoms in the basal plane occurs along the path O1 → T1 → O2 → O2 → T1 → O1, and oxygen can also diffuse from one basal plane into another. On the whole, the highest barrier that limits oxygen diffusion in the Ti_3Al alloy at a low oxygen content is 2.42 eV and corresponds to the elementary path O1 → T1. The calculated temperature diffusion coefficient and the activation energy along the [0001] direction and normal to it are 1.99 and 1.97 eV, which agrees with the experimental data from [19]. On the whole, the energy barriers of diffusion from preferred sites increase with the titanium content in a Ti–Al alloy; therefore, these sites can serve as oxygen traps, which retards oxygen diffusion and hinders aluminum oxidation. These results can be used to understand the nature of the oxygen diffusion rate in Ti–Al alloys and the oxidation of metallic systems.

ACKNOWLEDGMENTS

The numerical calculations were carried out on the SKIF-Cyberia supercomputer in Tomsk State University and using the resources of the Supercomputer Center of Moscow State University [61].

This work was supported in part by the Russian Foundation for Basic Research (project no. 14-02-91150_GFEN), project 23.1.2 of the Institute of Strength Physics and Material Science, and also by the Tomsk State University Competitiveness Improvement Program.

REFERENCES

1. Z. Li and W. Gao, in *Intermetallics Research Progress,* Ed. by Y. N. Berdovsky (Nova Science, New York, 2008), p. 1.
2. F. Motte, C. Coddet, P. Sarrazin, et al., Oxid. Met. **10**, 113 (1976).
3. I. Polmear, *Light Alloys: From Traditional Alloys to Nanocrystals* (Elsevier, Amsterdam, 2005; Tekhnosfera, Moscow, 2008).
4. A. Rahmel and P. J. Spencer, Oxid. Met. **35**, 53 (1991).
5. K. L. Luthra, Oxid. Met. **36**, 475 (1991).
6. P. Kofstad, *High Temperature Corrosion* (Elsevier Science, London, 1988).
7. T. G. Avanesyan, Cand. Sci. (Chem.) Dissertation (Natl. Univ. Sci. Technol. MISiS, Moscow, 2014).
8. V. Maurice, G. Despert, S. Zanna, et al., Acta Mater. **55**, 3315 (2007).
9. S.-Y. Liu, S. Liu, D. Li, et al., Phys. Chem. Chem. Phys. **14**, 11160 (2012).
10. M. R. Shanabarger, Appl. Surf. Sci. **134**, 179 (1998).
11. M. Ramachran, D. Mantha, C. Williams, et al., Metal. Mater. Trans. A **42**, 202 (2011).
12. G. M. Hood, J. Nucl. Mater. **135**, 292 (1985).
13. H. Nakajima, G. M. Hood, and R. J. Schultz, Philos. Mag. B **58**, 319 (1988).
14. H. Nakajima and M. Koiwa, ISIJ Int. **31**, 757 (1991).

15. H. Nakajima, K. Yusa, and Y. Kondo, Scr. Mater. **34**, 249 (1996).
16. J. Rüsing and Chr. Herzig, Intermetallics **4**, 647 (1996).
17. J. Breuer, T. Wilger, M. Friesel, et al., Intermetallics **7**, 381 (1999).
18. Chr. Herzig, M. Friesel, D. Derdau, et al., Intermetallics 7, 1141 (1999).
19. Y. Koizumi, M. Kishimoto, Y. Minamino, et al., Philos. Mag. **88**, 2991 (2008).
20. M. J. Gillan, J. Phys. C **20**, 3621 (1987).
21. G. A. Voth, D. Chandler, and W. H. Miller, J. Chem. Phys. **91**, 7749 (1989).
22. D. E. Jing and E. A. Carter, Phys. Rev. B **70**, 064102 (2004).
23. X. L. Han, Q. Wang, D. L. Sun, et al., Int. J. Hydrogen Energy **34**, 3983 (2009).
24. D. Connétable, J. Huez, É. Andrieu, et al., J. Phys.: Condens. Matter **23**, 405401 (2011).
25. A. Yu. Kuksin, A. S. Rokhmanenkov, and V. V. Stegailov, Phys. Solid State **55**, 367 (2013).
26. Z.-S. Nong, J.-C. Zhu, X.-W. Yang, et al., Comput. Mater. Sci. **81**, 517 (2014).
27. A. V. Bakulin, S. S. Kulkov, S. E. Kulkova, et al., Int. J. Hydrogen Energy **39**, 12213 (2014).
28. A. V. Bakulin, S. S. Kulkov, and S. E. Kulkova, Phys. Solid State **56**, 1261 (2014).
29. S. S. Kulkov, A. V. Bakulin, and S. E. Kulkova, J. Exp. Theor. Phys. **119**, 521 (2014).
30. J. W. Wang and H. R. Gong, Int. J. Hydrogen Energy **39**, 6068 (2014).
31. A. V. Bakulin, T. I. Spiridonova, S. E. Kulkova, et al., Int. J. Hydrogen Energy **41**, 9108 (2016).
32. H. Wu, *Oxygen Diffusion Through Titanium and Other hcp Metals* (Univ. of Illinois, Urbana, IL, 2013).
33. H. Li, S. Wang, and H. Ye, J. Mater. Sci. Technol. **25**, 569 (2009).
34. S.-Y. Liu, J.-X. Shang, F.-H. Wang, et al., Phys. Rev. B **79**, 075419 (2009).
35. L. Wang, J.-X. Shang, F.-H. Wang, et al., Acta Mater. **61**, 1726 (2013).
36. C. E. Kulkova, A. V. Bakulin, Q. M. Hu, and R. Yang, J. Exp. Theor. Phys. **120**, 257 (2015).
37. S. E. Kulkova, A. V. Bakulin, Q. M. Hu, et al., Comput. Mater. Sci. **97**, 55 (2015).
38. A. M. Latyshev, A. V. Bakulin, C. E. Kulkova, Q. M. Hu, and R. Yang, J. Exp. Theor. Phys. **123**, 991 (2016).
39. A. Bakulin, A. Latyshev, and S. Kulkova, Solid State Phenom. **258**, 408 (2017).
40. L.-J. Wei, J.-X. Guo, X.-H. Dai, et al., Surf. Rev. Lett. **22**, 1550053 (2015).
41. L. J. Wei, J. X. Guo, X. H. Dai, et al., Surf. Interface Anal. **48**, 1337 (2016).
42. T. Hong, T. J. Watson-Yang, X.-Q. Guo, et al., Phys. Rev. B **43**, 1940 (1991).
43. D. Sornadurai, B. Panigrahi, and Ramani, J. Alloys Compd. **305**, 35 (2000).
44. D. Music and J. M. Schneider, Phys. Rev. B **74**, 174110 (2006).
45. Y. A. Bertin, J. Parisot, and J. L. Gacougnolle, J. Less-Common Met. **69**, 121 (1980).
46. P. E. Blöchl, Phys. Rev. B **50**, 17953 (1994).
47. G. Kresse and J. Joubert, Phys. Rev. B **59**, 1758 (1999).
48. G. Kresse and J. Hafner, Phys. Rev. B **48**, 13115 (1993).
49. G. Kresse and J. Furthmüller, Comput. Mater. Sci. **6**, 15 (1996).
50. J. P. Perdew, K. Burke, and M. Ernzerhof, Phys. Rev. Lett. **77**, 3865 (1996).
51. G. Henkelman, B. P. Uberuaga, and H. Jónsson, J. Chem. Phys. **113**, 9901 (2000).
52. P. Villars and L. D. Calvert, in *Pearson's Handbook of Crystallographic Data for Intermetallic Phases,* 2nd ed. (ASM Int., Materials Park, OH, 1991).
53. K. Tanaka, K. Okamoto, H. Inui, et al., Philos. Mag. A **73**, 1475 (1996).
54. C. Y. Jones, W. E. Luecke, and E. Copland, Intermetallics **14**, 54 (2006).
55. Y. Wei, H.-B. Zhou, Y. Zhang, et al., J. Phys.: Condens. Matter **23**, 225504 (2011).
56. C. J. Rosa, Metall. Trans. **1**, 2517 (1970).
57. M. Dechamps and P. Lehr, J. Less-Common Met. **56**, 193 (1977).
58. D. David, G. Beranger, and E. A. Garcia, J. Electrochem. Soc. **130**, 1423 (1983).
59. V. B. Vykhodets, S. M. Klotsman, T. E. Kurennykh, et al., Fiz. Met. Metalloved. **68**, 723 (1989).
60. F. L. Bregolin, M. Behar, and F. Dyment, Appl. Phys. A **86**, 481 (2007).
61. Vl. V. Voevodin, S. A. Zhumatii, S. I. Sobolev, et al., Otkryt. Sist., No. 7, 36 (2012).

Translated by K. Shakhlevich